Dalton Transactions

Accepted Manuscript

ROYAL SOCIETY OF CHEMISTRY

www.rsc.org/dalton

Dalton Transactions

ARTICLE

Platinum Complexes Bearing Normal and Mesoionic *N*-Heterocyclic Carbene Based Pincer Ligands: Syntheses, Structures, and Photo-Functional Attributes

Received 00th December 2015,
Accepted 00th January 20xx

DOI: 10.1039/x0xx00000x

www.rsc.org/

Abbas Raja Naziruddin, Chen-Shiang Lee, Wan-Jung Lin, Bing-Jian Sun, Kang-Heng Chao, Agnes Hsiu Hwa Chang*, and Wen-Shu Hwang*

Platinum complexes featuring pyridine *bis*-*N*-heterocyclic–imidazol-2-ylidene/–mesoionic-triazol-5-ylidene donors as pincer ligands and chloro (–Cl), acetonitrile (–$NCCH_3$) or cyano (–CN) groups as auxiliary ligands are prepared as highly strained organometallic phosphors. X-ray structures of four of these complexes confirm a distorted square planar geometry, where the pincer ligand and its mesityl wingtips occur in a twisted conformation to each other. Electrochemical and photo physical characterization have been carried out and the experimental results are interpreted with the aid of density functional theory calculations. Emission responses of complexes under exposure to different vapors and mechanical shear are reported. Notably, the platinum complex featuring pyridine *bis*-imidazol-2-ylidene and a weakly donating acetonitrile auxiliary ligand exhibited strong aquachromic and mechanochromic emission responses, showing color changes from sky blue to green or yellow-green.

Introduction

Transition metal complexes of *N*-heterocyclic carbene ligands (NHCs) have found vast application in molecular catalysis,[1] material science[2] and medicine.[3] Recent researches have also coupled their photo emissivity with anti-cancer activity and demonstrated their potential use towards lifesaving *chemo-theranostic* treatment.[4] Bright emission of such complexes can be attributed to the presence of heavy atom like platinum, which induces strong spin-orbit-coupling.[5] Equally important is the strong σ donating ability of NHC ligands, which could facilitate the separation of triplet-emissive states from the non-emissive ligand field states (LF) to render long-lived radiative lifetimes.[6] Further, tuning of electronic structure (and photo physics) of such complexes is possible through facile modifications *via* use of different NHCs[7] and co-ligands of varying donor strengths.[6e, 8] Such organometallic complexes have shown to be useful in functional areas like organic light emitting diodes (OLEDs), sensor devices, or as bio-molecular probes.[3, 6c, 9]

Square planar platinum complexes featuring pincer type ligands possess rigid structural framework, which resist the vibrational deactivation of the excited states.[10] In addition, changes conferred to their local environment can also influence the emission characteristics. Such emissive responses often arise from the interaction of the d_z^2 orbital lying normal to the coordination plane with different solvent molecules or platinum centre of the neighbouring molecules.[3, 11] Few recent studies have manifested this property for potential uses in solid-state sensors to detect volatile organic vapor or mechanical shear.[8, 11a, 12] However, reports of platinum complexes featuring NHC based ligands exhibiting vapochromic or mechanochromic attributes are relatively rare,[12b, 12c] as compared to those bearing *N*-donors or the ones bearing anionic alkylidene/phenylene donor sets.[12d-g, 13] In an earlier contribution, we have shown the aqua chromic luminescence switching behaviour of platinum complex featuring CNC type pincer ligand, where the classical imidazol-2-ylidene donors was used as terminal carbene donor and CO was the auxiliary ligand.[12b]

Structural modification arising from the substitution of normal NHC with an abnormal carbene donor will have a pronounced effect on the electron donor ability of the pincer ligand.[14,15] Moreover a class of 1,2,3-triazol-5-ylidene based mesoionic carbene donors (MIC) which could be accessed through facile [2+3] cycloaddition of an alkyne with an azide,[16] have demonstrated stronger donor properties than their normal NHC congeners.[17] Platinum(II) complexes of these MIC donors have been reported before in mono nuclear[18] and poly nuclear[19] forms. Even though the pincer ligands featuring two

[a]National Dong Hwa University-Hualien 97401, Taiwan (ROC)
E-Mail: hws@mail.ndhu.edu.tw
†Electronic Supplementary Information (ESI) available:
Crystallographic information files are deposited at the CCDC database with the indexing numbers of 1438423–1438427. Experimental crystallographic details, computed transitions (TD-DFT) in the form of a table and combined molecular coordinates files of the optimized singlet geometries are given. This material is available free of charge via the Internet at http://pubs.rsc.org. See DOI: 10.1039/b000000x/

MIC donors linked to a central pyridine[9b, 20] or carbazolide spacers[21] are known, only their respective ruthenium(II) or copper(II) complexes are available in the literature. To the best of our knowledge, platinum complexes featuring pyridine *bis*-MIC donors is unknown to date.

Herein, we report the preparation of platinum complexes of type $[Pt^{NHC/MIC}(CNC)^{NHC/MIC}–L]$ (*L* = Cl, $NCCH_3$ and CN). X-ray structures, spectroscopic properties and redox potentials are measured and density functional theory calculations (DFT) are performed in support of experimental results. In addition, complexes are also screened for photo functional attributes of vapo/ and mechanochromism and results are reported herein.

Results and Discussion

Syntheses and Characterization

The precursor complex **1** was obtained from the reaction of 2, 6-*bis*(1-mesitylimidazolium-3-yl)pyridine dibromide,[1d] with Ag_2O and K_2PtCl_4 in DMSO at 100 °C, as previously reported.[12c] Reaction of **1** with $AgPF_6$ in acetonitrile or with AgCN in dichloromethane gave **2** (73%) or **3** (81%) respectively in good yields (Scheme **1**). Protons of the central pyridine rings of coordinated pincer ligand in **1**·PF_6, **2** and **3**, are detected as doublet in the range of δ 7.91–8.15 ppm and as a triplet in the range of δ 8.66–8.47 ppm ($J_{H-H} \approx 8.4$ Hz) in the ^{1}H NMR. These signals appeared in a relative-downfield region, as compared to the free ligand precursor. Noticeably, the ^{1}H NMR of **3** showed a relative up field shift of mesityl–H resonance which occurred at δ 6.99 ppm as compared to those of **2** (δ 7.14 ppm). Further, an additional singlet at δ 1.82 ppm in the ^{1}H NMR indicated the presence of coordinated acetonitrile moiety in **2**. The carbenoid-carbon atom of **1**·PF_6 and **2** are diagnosed at δ 168.9 and 166.8 ppm respectively in ^{13}C NMR. The carbenoid carbon resonance of the cyano bound complex **3** occurred at δ 169.4 ppm, whereas the coordinated cyanide resonance was detected at 124.8 ppm in the ^{13}C NMR. In addition, the IR spectra showing C≡N stretching band at 2143.1 cm^{-1} confirmed the presence of coordinated cyanide in **3**.

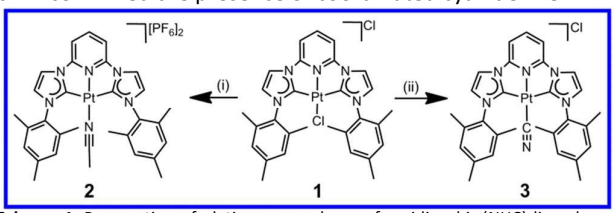

Scheme 1. Preparation of platinum complexes of pyridine *bis*-(NHC) ligands and co-ligands of acetonitrile and cyanide donors. (i) $AgPF_6$/ acetonitrile; (ii) AgCN.

Alternatively, platinum complexes of CNC pyridine *bis* MIC ligands are prepared *via* a different approach (Scheme **2**). First, the tetrachloroplatinate salt was prepared by reacting an excess stoichiometry of K_2PtCl_4 with $H_2^{MIC}(CNC)^{MIC}[BF_4]_2$ in an aqueous–acetonitrile solution. ^{1}H NMR of the $H_2^{MIC}(CNC)^{MIC}[PtCl_4]_2$ salt was characterized by a relative downfield shift of C^5–*H* signals to 10.01 ppm as compared to the tetra fluoroborate salt (δ 9.02 ppm). Subsequently, the reaction of $H_2^{MIC}(CNC)^{MIC}[PtCl_4]_2$ with silver oxide under elevated temperature of 140 °C gave the platinum complex **4** (32.2%). **4** was transformed into acetonitrile bound **5** (86%) and cyano bound **6** (81%), upon reacting with $AgPF_6$ or AgCN respectively at ambient temperature.

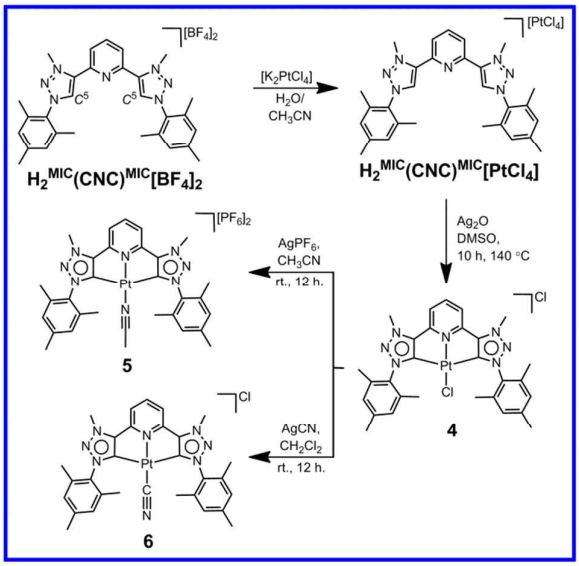

Scheme 2. Syntheses of Platinum complexes bearing mesoionic pincer ligands.

^{1}H NMR spectra of complexes are devoid of C^5–*H* resonances at δ 10.01 ppm. Analogous to complexes bearing pyridine *bis*-imidazol-2-ylidene donors, the signals of pyridyl–*H* in **4**–**6** are clearly detected as two sets of peaks, one as a triplet in the range of δ 8.39–8.44 ppm and the other as a doublet in the range of δ 8.04–8.16 ppm ($J_{H-H} \approx 8.0$ Hz) in ^{1}H NMR. An additional peak at δ 1.30 ppm in the ^{1}H NMR of **5** is ascribed to the coordinated acetonitrile moiety. The ^{13}C NMR resonance of C^5 atom of $H_2^{MIC}(CNC)^{MIC}[PtCl_4]$ observed at 131.1 ppm disappeared in complexes **4**, **5** and **6**. Concomitantly additional signals appeared at δ 120.6, 121.9, and 121.2 ppm for **4**, **5** and **6** respectively in the ^{13}C NMR. These signals compare well with the C^5–Pt resonances of previously known platinum complexes of abnormal/mesoionic carbene ligands.[15, 22] In addition, IR spectra of **6** showing the coordinated cyanide stretching at lower frequencies of 2131.0 cm^{-1} than **3** (2143.1 cm^{-1}), indicated a stronger electron donor ability of mesoionic carbene donors. Further confirmation of the identity and the analytical purity of these complexes are attained through mass spectra and elemental analyses.

Structural Analyses

Single crystals of **1**, **3** and **4** suitable for X-ray diffraction could not be obtained directly. Therefore, hexafluorophosphate salts of **1**, **3** and **4** are prepared. X-ray quality crystals were obtained by slow diffusion of diethyl ether into acetonitrile solutions of **1**·PF_6 and **2**. Dissolving the powder samples of **3**·PF_6 in a mixture of dichloromethane and methanol (4:1, *V*:*V*) and subsequent diffusion of diethyl ether vapor, gave single crystals, which co-crystallized with the molecules of dichloromethane. Alternatively, slow diffusion of diethyl ether into a mixture of acetone and acetonitrile (3:1,

V:*V*) containing **4**·PF_6 gave its single crystals. Crystal structures of **2** and **3**·PF_6 are depicted in Fig. **1** and those of **4**·PF_6 and **1**·PF_6 are shown in Fig. **2** and Fig. **S1** respectively. Selected metric parameters are listed in the caption and the experimental crystallographic details are listed in Table **S1** (Supporting Information).

Crystal structures of complexes confirm the pincer type coordination of pyridine *bis*-NHC/MIC ligand to the platinum(II) centre in a quasi-planar disposition. Either a halide, acetonitrile or a cyanide donor completes the fourth coordination site to render pseudo square planar geometry.

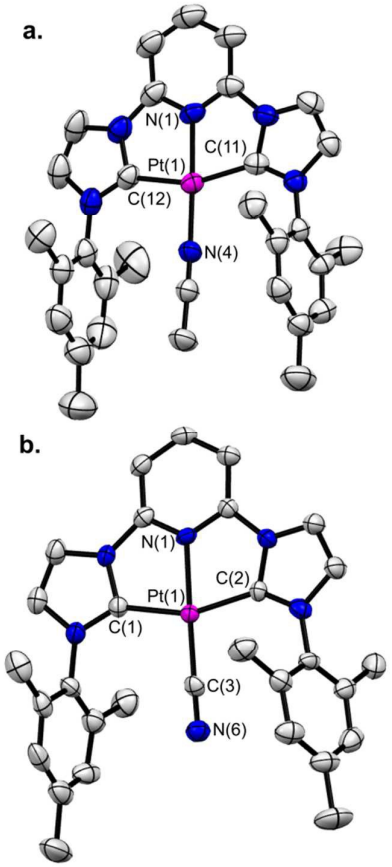

Fig. 1. Molecular structure of platinum complexes **2** and **3·PF$_6$** are depicted with 50% probability ellipsoids with counter anions, hydrogen atoms, and solvent molecules omitted for clarity. Important bond distances (Å) and angles (°) are summarized. For **2**: Pt(1)—N(1) 1.980(4), Pt(1)—C(11) 2.026(6), Pt(1)—C(12) 2.014(7), Pt(1)—N(4) 1.980(4), C(11)—Pt(1)—C(12) 159.0(2), N(1)—Pt(1)—N(4) 177.3(2). For **3**: Pt(1)—N(1) 2.010(1), Pt(1)—C(1) 2.015(9), Pt(1)—C(2) 2.004(8), Pt(1)—C(3) 1.930(2), C(1)—Pt(1)—C(2) 157.7(3), N(1)—Pt(1)—C(3) 177.1(7).

1·PF_6 exhibited the shortest Pt–C_{NHC} bond distance of 1.998(3) Å, whereas the one in **2** measuring 2.026(6) Å was found to be the longest amongst complexes described herein. These bond distances are comparable to previously reported metric parameters of Pt–C_{NHC} bonds (≈ 2.01 Å).[12c] However in comparison to complexes featuring relatively less strained pincer ligands (1.975 Å),[12b] the Pt–C_{NHC} bond lengths of **1**·PF_6, **2** and **3**·PF_6 are slightly longer (1.998(3)–2.026(7) Å).

The Pt–L_{aux} bond distances are observed in the range of 1.963(6)–2.286(1) Å, with the –Cl bound **1**·PF_6 and the cyano bound **2** featuring the longest and the shortest values of 2.286(1) Å and 1.930(2) Å respectively. The Pt–N_{CNC} bond distances and the observed distortions in C_{NHC}–Pt–C_{NHC} bite angles (157.8(2)–159.0(2)°) of these complexes fall well within a comparable range to other platinum complexes featuring terdentate *N*-donor sets.[12e, 13b, 23] A twisted conformation between the mesityl-wingtips and the coordination plane of the platinum centre is evident from the measured torsion angles of 93.90° and 93.05° in **1**·PF_6, 91.25° and 95.30° in **2**, and 103.12° and 107.40° in **3**·PF_6.

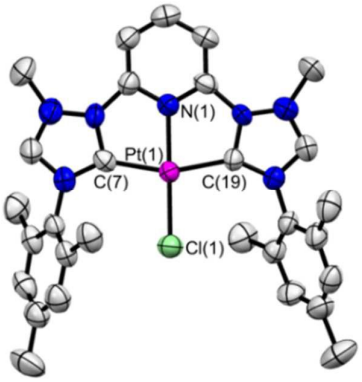

Fig. 2. Crystal structure of **4·PF$_6$** is depicted with 50% probability ellipsoids with counter anions, hydrogen atoms, and solvent molecules omitted for clarity. Important bond distances (Å): Pt(1)—N(1) 2.012(7), Pt(1)—C(7) 1.998(8), Pt(1)—C(19) 2.009(9), Pt(1)—Cl(1) 2.279(2); and angles (°) C(7)—Pt(1)—C(19) 159.5(4), C(7)—Pt(1)—N(1) 79.7(3), N(1)—Pt(1)—Cl(1) 179.1(2), N(1)—Pt(1)—C(19) 79.8(3).

4·PF_6 (Fig. **2**) and **1**·PF_6 (Fig. **S1**, ESI), featuring different pincer ligands of MIC and NHC donors respectively, however bound to the same auxiliary ligand (–Cl), are compared. Structural analysis reveal that the average Pt–C_{NHC} bond distance of 2.004 Å in **4**·PF_6 is nearly identical to those of **1**·PF_6. However the Pt–$N_{pyridyl}$ bond distance of **1**·PF_6 (1.973 Å) is shorter than those in **4**·PF_6 (2.012 Å). On the contrary, the *trans* lying Pt–Cl bond length of **1**·PF_6 (2.286(1) Å) is slightly longer than those in **4**.PF_6 (2.279(2) Å). An apparent square planar distortion is also evident from the crystal structure of **4**·PF_6, in spite of a relatively wider C_{NHC}–Pt–C_{NHC} bite angle of 159.5(4)°, than their normal NHC counterpart. Further, large torsion angles of 111.97° and 104.84° between the mesityl rings and the plane of the pincer ligands also confirm a twisted conformation between them.

Large torsion angles in **1**·PF_6–**4**·PF_6 forbids the inter-molecular Pt···Pt interactions in the crystalline state. However, the nearest cationic fragments at perpendicular disposition of pincer-ligands often resulted in C–*H*···π interactions. **1**·PF_6 featured C–*H*···π contact of 3.446 Å between C^{Mes}–*H* and a pyridine-*C*. Whereas secondary interactions in **4**·PF_6, that features MIC based pincer ligand are relatively weak. The asymmetric unit of **3** comprise two pairs of cations with one at the core and the other at the periphery. Pincer ligand of cationic fragments of the same pair is arranged in a parallel conformation, while the ones of opposite pair feature a perpendicular arrangement. This molecular arrangement of **3** gave short C–*H*···π contact, with a mean distance of 2.732 Å between the NHC backbone (C–*H*) and the mesityl ring.

Dalton Transactions

ARTICLE

Table 1: Summary of electronic absorptions and redox potentials of selected complexes.

	Absorption	Redox Potential		Emission			
	λ_{max}(nm) (ε/$M^{-1}cm^{-1}$)	$E_{1/2}$ (V) (oxidation)	$E_{1/2}$ (V) (reduction)	Solution		Solid	
				λ_{max}[d] (nm)	τ[d] (μs)	λ_{em}[e](nm)	τ (μs)[e]
1	273 (23210), 309 (6779)–324 (5370),[c] 366 (4021)–385 (3970) and 409–430 (< 1300)[a]	+1.10	–0.83	559	3.20	523	6.81
2	263 (15075), 315 (6942), 383 (1500) and 406 (< 1000)[b]	+1.19	–0.86	455, 472	3.55	483	6.44
3	264 (8975), 291 (6922)[c], 361 (1866),[c] 387–412 (< 1000)[a]	+1.22	–0.82	410, 436, 467	4.42	445, 468, 491[c]	6.88
4	245 (37558), 290 – 350 (21772), 365–401 (< 5000)[c]	+1.10	–0.85	504	6.93	493,[c] 527, 559[c]	5.78
5	243 (25496), 286 (15550), 317 (10893)	+1.15	–0.83	494	1.68	493,[c] 530	7.32
6	227 (16442), 260–287 (8747), 308 (2804)–375 (≈ 1000)	+1.12	–0.83	490, 522	5.58	519, 550[c]	5.25

Absorption spectra were recorded in dichloromethane[a] or methanol[b] solutions in the concentration range of 2.43 $\times10^{-4}$ – 7.11$\times$ 10^{-5} M; shoulder;[c] solution state emission;[d] solid state emission.[e] Excitation wavelength for different complexes: **1**: 400[d] and 374 nm[e]; **2**: 318[d] and 397 nm[e]; **3**: 358[d] and 356 nm[e]; **4**: 330[d] and 371[e]; **5**: 374[d] and 349nm[e]; **6**: 335[d] and 374 nm[e].

NHC ligands of adjacent cationic fragments of **2** occur in close proximity with the shortest C–*H*$\cdots\pi$ contact of 3.271 Å. In addition, **2** and **2**·H_2O also exhibited several hydrogen bonding interactions, where the donor sites are the protons of NHC backbone, coordinated acetonitrile and mesityl-methyl fragments and the acceptor sites are the fluorine atoms of PF_6 anion.

The strongest hydrogen bonding interaction in **2** was observed between the NHC (C–*H*) of the cation and the PF_6 anion with donor–acceptor distance of 2.243 Å (< sum of *vander waals* radii 2.5–2.7 Å).[24] Four cationic fragments within the asymmetric units of **2**·H_2O occupy the corners of a parallelogram, with diagonal pairs in a head to tail arrangement. **2**·H_2O exhibited an average C–*H*$\cdots\pi$ distance of 2.720 Å with the shortest one measuring only 2.611 Å between the NHC back bone (C–*H*) and the adjacent mesityl ring. As in **2**, the most prominent hydrogen bonding interaction of **2**·H_2O, was also observed between NHC (C–*H*) and the fluorine atom of PF_6 anion (2.311 Å). In addition, short donor–acceptor contacts of 2.457 and 2.574 Å are also detected between the pyridine–H and the PF_6 anion of **2**·H_2O.

Spectroscopy, Electrochemistry and Computational Studies

Absorption spectra of complexes **1–3** and **4**–**6** are shown in Fig. **3** and Fig. **4** respectively and the data is listed in Table **1**. Ground state structures of **1**–**6** are optimized using B3LYP[25] functional within the SDD basis set,[26] and the computed molecular geometries for vacuum is provided as a separate molecular coordinates file in ·xyz format (ESI). Optimized S_0 structures are subjected to time dependent density-functional theory calculations (TD-DFT) to estimate the vertical transition energies and oscillator strengths (Table **3.1**). Orbital diagram of HOMO – 14 to LUMO + 14 levels are shown in Table **S2.1–S2.6** for complexes **1–6**.

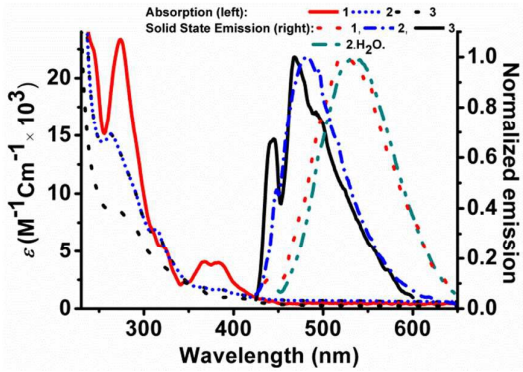

Fig. 3. Absorption spectra of **1**, **2** and **3** measured in solution state (left) and emission spectra of **1**, **2**, and **3** and **2**·H_2O recorded in the solid-state (right).

Higher-energy (HE) absorption bands with large molar extinction coefficients are observed at ≈ 260 nm for complexes **1**–**3**, that feature pyridine *bis*-NHC donors. These bands are attributed to electronic excitations arising from the low-lying HOMO – *n* levels into the LUMOs where *n* = 9, 8 and 10 for **1**, **2**, and **3** respectively. However, in the series of complexes featuring pyridine *bis*-MIC donors (**4**–**6**), these HE bands become even-more energetic and involve more than one type of electronic excitations. The absorption band peaking at 245 nm in **4** is attributed to an admixture of HOMO – *n* (*n* = 11, 8) → LUMO + 1 and HOMO – 9 → LUMO excitations. Whereas, the HE band of **5** (243 nm) originates from an admixture of HOMO – 7 → LUMO + 4 and HOMO – 8 → LUMO +1 excitation. These HE excitations can be ascribed to metal perturbed intra ligand charge transfer excitations (MP-^{1}ILCT).[27]

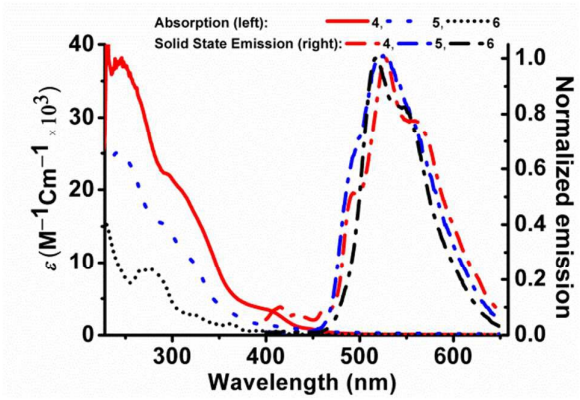

Fig. 4. Absorption spectra of complexes **4**, **5**, and **6** measured in solution state (left) and emission spectra in solid states.

Moderately intense absorption bands observed in the spectral window of 309–324 for **1** correspond to HOMO – 6 → LUMO + 1 excitations. However, similar absorption band of **2** peaking at 315 nm is attributed to an admixture of HOMO – *n* → LUMO, where *n* = 5 and 7; and HOMO – 4 → LUMO + 1 excitations. Absorption bands of relatively weaker intensity detected in complexes **1**–**3** in the range of 360–410 nm are attributed to HOMO – 4 → LUMO excitation.

Broad absorption shoulder detected for **4** between 290–350 nm arises from an admixture of electronic excitations of HOMO – 11 → LUMO + 1 and HOMO – 6 → LUMO + 2. A relatively less intense peak observed for **5** at 286 nm is devoted to the electronic transition from HOMO – 9 into the LUMO level. TD-DFT calculations suggest that weaker intensity absorption band of **6** (260–300 nm) arises from combined intensities of two different electronic excitations at 277 and 281 nm. Absorption at 277 nm arises from an admixture of HOMO – *n* → LUMO, where *n* = 9, 11; and HOMO – 6 → LUMO + 3, whereas the one at 281 nm correlates with an admixture of HOMO – 9 → LUMO + 1 and HOMO – 6 → LUMO + 2 excitations. As the involved molecular orbitals (MOs) tend to be largely mixed, one could in general ascribe these lower energy electronic excitations to mixed metal-to-ligand-charge transfer bands (*mixed* ^{1}MLCT).[28] Weakly intense–lower energy absorption tails detected in the range of 365–401 and 308–375 nm in **4** and **6** respectively, and above 317 nm in **5** could be ascribed to electronic-charge transfer originating from their respective HOMO – 6 levels, however into distinct final states of LUMO + 1, LUMO + 2 or the LUMO in order.

DFT calculations indicate larger participitation of metal orbitals in the HOMOs of the complexes **4** and **6**, bearing MIC donors. Isodensity surface plots of HOMOs of complexes featuring different pincer ligands but the same auxiliary ligands of –Cl (**1** and **4**) or the –CN (**3** and **6**) donors clearly show a relatively larger orbital weightage upon the platinum centre in **4** (15.6%) and **6** (1.5%), than those of **1** (9.7%) and **3** (0.3%) respectively. However, irrespective of carbene donors HOMOs of the acetonitrile bound **2** and **5** (0.05%) show nearly neglegible participation of metal centre (Fig. **5** and Table **S3.2**).

Cyclic voltammograms of complexes **1–6** recorded from deaerated acetonitrile solutions showed quasi-reversible oxidation waves in the range of + 1.10 to 1.22 V ($E_{ox}^{1/2}$, Table **1**). Comparing complexes of identical net charges and counter ions, but different pincer ligands (i.e., **2** *vs* **5** and **3** *vs* **6**) indicates that introducing MIC donors into the inner sphere of the platinum(II), tend to lower the oxidation potential. Stronger electron donor ability of the MIC donors is reasoned for this behaviour.[29] However, the oxidation potential of **4** bearing two MIC donors is identical to those of **1** ($E_{ox}^{1/2}$ = + 1.10 V). This can be attributed to the fact that HOMO of **1** involves a relatively larger participation of ligand orbitals, while those of **4** is associated with more of metal. An admixture of ligand/co-ligand/metal centred oxidation could be reasonably assigned to the anodic waves of **1** and **4**. Related anodic process involving ligand, co-ligand and the metal centre (Pt^{II} to Pt^{III}) has been previously described for platinum complexes bearing terdentate *N*-donor sets. These anodic potentials were reported in the electrochemical window of + 0.60 to +1.75 V.[23b, 30] Unlike **1** and **4**, for complexes **2**, **3**, **5**, and **6** showing maximal participation of pincer ligand in the HOMO levels, a more ligand centred oxidative process is ascribed.

The facile oxidative process of the chloride bound complex **1** ($E_{ox}^{1/2}$ = + 1.10 V), could be attributed to its mono cationic nature, as compared to the di-cationic **2** ($E_{ox}^{1/2}$ = + 1.19 V). Even though both of the complexes **1** and **3** are mono cationic, the relative sluggishness of the oxidative process in the latter could be attributed to the effective π-accepting nature of the –C≡N ligand ($E_{ox}^{1/2}$ = + 1.22 V). Amongst complexes **4**–**6**, the most sluggish oxidative process was detected in the dicationic **5** ($E_{ox}^{1/2}$ of + 1.15 V). Whereas the oxidative wave of the monocationic **6** ($E_{ox}^{1/2}$ = + 1.12 V) occurred at midway between those of **4** and **5**. A compensatory electron donation from two MIC donors of the pincer ligand somewhat annuls the electron withdrawing effect of C≡N ligand in **6**, thus avoiding further increase of its oxidative potential.

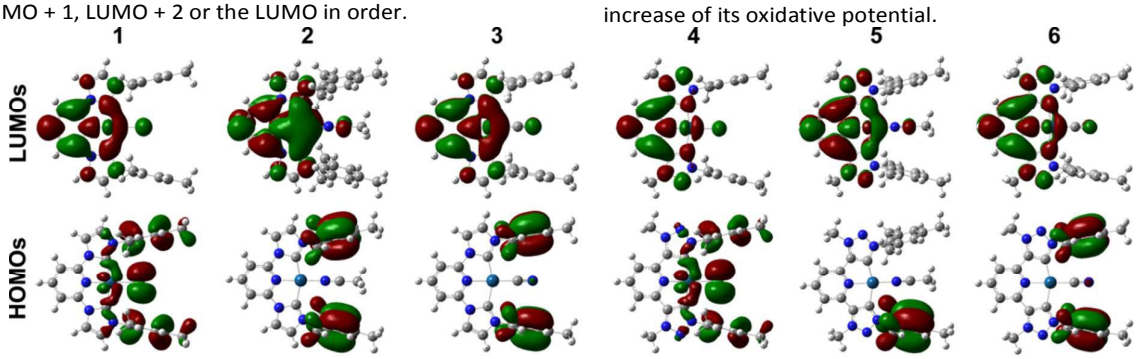

Fig. 5. View of computed HOMO and LUMO levels of the complexes **1**–**3** and **4**–**6** in the ground states.

Dalton Transactions

ARTICLE

DFT computed LUMOs of **1**–**6** are mainly centred upon the pyridine fragment of the pincer ligand, with minimal participation of metal orbitals. Reduction couple of complexes **1**–**6** in the range of –0.82 to –0.86 V ($E_{red}^{1/2}$) mainly involve the pyridine ring.[31] Slight lowering of reduction potentials of **3** relative to **1** and **2** could be ascribed to the presence of π-accepting cyano ligand. As expected, we also observed a relative lowering of $E_{red}^{1/2}$ of **6** in comparison to **4**, but not relative to **5**. This relatively less responsive π-electron withdrawing effect in **6** could be attributed to the nature of its LUMO, which shows a significantly lower contributions of –CN (0.5%) as compared to those of **3** (1.71%). In addition, weak influence of co-ligands on cathodic potentials are also more evident from their low orbital weightages in the LUMO levels with –Cl bound **1** and **4** showing 1.79 and 1.28% or the $-NCCH_3$ bound **2** and **5** showing 3.2 and 0.1% respectively (Table **S3**).

Emission Characteristics

Neat samples of **1** emitted green (523 nm), whereas **2** emitted sky blue (483) and **3** emitted blue light (468 nm) in the solid state. As compared to emission spectra recorded from acetonitrile solutions, solid-samples of **2** and **3**-exhibit bathochromic shift of their emission maxima along with the loss of fine structures (Fig. **3** and **S3a**). Complexes **4**–**6** emitted green light, with emission maxima of **4** (527 nm) and **5** (530 nm) close to each other. Further, **4** exhibited two well-defined shoulders, one at 493 nm and the other at 559 nm; whereas **5** displayed only a weak HE shoulder at 493 nm. Solid-state emission of **6** was observed as a featureless band peaking at 519 nm, with the loss of solution state fine structures at 490 and 522 nm, however along with a shoulder at 550 nm (Fig. **4** and **S3b**).

The microsecond regimes of excited state life times of complexes **1**–**6**, both in solution (1.68–6.93 μs) and in the solid state (3.55–7.32 μs), indicate that these emission originate from triplet manifold, which confirms phosphorescence ($T_1 \rightarrow S_0$) (Table **1**).[32] Comparing the solution and solid-state emission spectra, the latter are often observed as featureless bands. Clear loss of fine structure is more evident in **2** and **6**. In addition, emission bands exhibit large bathochromic shift in solid state. These solid-state emission bands can be reasonably ascribed as metal-ligand charge transfer in nature (^{3}MLCT),[33] whereas the one in **3**, showing vibronic bands even in the solid state are ascribed to an admixture of ^{3}MLCT and ^{3}LLCT.

Vapochromic and Mechanochromic Attributes

Upon exposure to moisture for a period of two hours or left under air for one day, the original sky blue emission color of **2** transforms to green (*Vide infra*). The reverse transformation of green to sky blue emission occurred when the solvent-chamber was re-filled with acetonitrile vapor. The emission-responses shown by **2** is due to its interaction with these solvent molecules.

The crystals of **2**, upon exposure to water vapor, absorbed a molecule of water, as confirmed by the results of elemental analysis (Anal. For $C_{31}H_{32}F_{12}N_6P_2Pt \cdot H_2O$: C 37.55; H 3.46; N 8.47. Found: C 37.44; H 3.52; N 8.52), which corresponded to **2**·H_2O. The X-ray structure of **2**·H_2O was also measured (Fig. **6**), even though the aquachromic exposure to some extent degraded the quality of the crystals. To our expectations and as indicated by elemental analyses data, we observed the exchange of lattice solvent of acetonitrile with a molecule of water. Furthermore, the detected water molecule was found at a proximally short and axially approachable Pt(1)–O(1) distance of 3.777 Å within the asymmetric unit. However, the structural study of the reverse process could not be performed as crystals underwent substantial degradation, when **2**·H_2O was exposed to acetonitrile vapor.

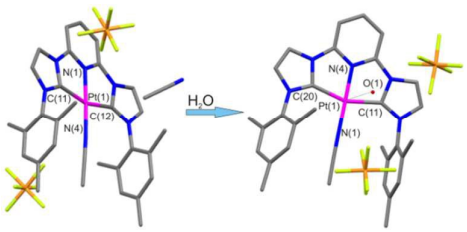

Fig. 6. Wire frame representation of molecular structure of **2**, shown along with a co-crystallized acetonitrile molecule (left) and with a molecule of water (right). Counter ions are shown, while, hydrogen atoms are omitted for clarity. Pt(1)···O(1) 3.809 Å.

The originally detected sky blue emission band of **2** which peaked at 483 nm in the solid state also underwent a clear bathochromic shift, upon exposure to other solvent vapors of methanol, tetrahydrofuran, acetonitrile, dichloromethane, hexane and water (Fig. **7**).

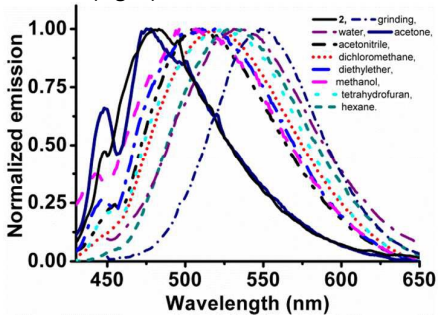

Fig. 7. Vapochromic and mechanochromic emission responses of **2**.

The vapochromic response of **2** is more pronounced for water molecules, as the new aqua chromic band (λ_{max} = 535 nm) is red-shifted by 52 nm from the original emission. Such a distinct change in the emission color from sky blue to green is only specific to water molecules. In contrast to [Pt(^{Mes}(CNC)^{Mes}CO]PF_6, which exhibited vapochromic color changes specific to acetone,[12c] under similar conditions **2** only showed an increase of the HE band intensity at 455 nm. In addition to vapochromic responses, **2** also exhibited stronger mechanochromic behaviour. Grinding of **2** using a mortar and pestle resulted in a sharp change in emission color. The resultant mechanochromic emission peaked at 549 nm (Fig. **6**). This color change from sky blue to greenish yellow ($\Delta\lambda_{em}$ = 66 nm) shown by **2** is very distinct and could be a valuable tool to detect the mechanical shear in materials.

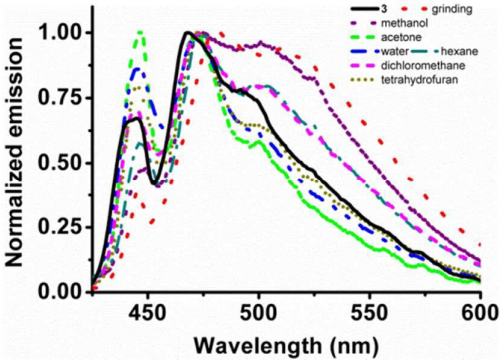

Fig. 8. Vapochromic and mechanochromic emission responses of **3**.

Fig. **8** summarizes the vapochromic and mechanochromic responses of **3**. The characteristic emission signatures left by different solvent vapors suggest the solvent specific interaction modes. Intensity of the emission band at 445 nm grew in the order of thf < water < acetone or decreased in the order of hexane < methanol. The emissive shoulder at 491 nm gained intensity along with a red shift to 502 nm. For the same solvent vapor, the order of intensity of this new peak followed a reverse trend as those of the higher energy band at 445 nm (acetone < water < thf < dichloromethane ≈ hexane < methanol). Grinding of **3** also resulted in bathochromic shifts of the highest intensity peak at 468 to 491 nm and the shoulder peak at 478 to 511 nm.

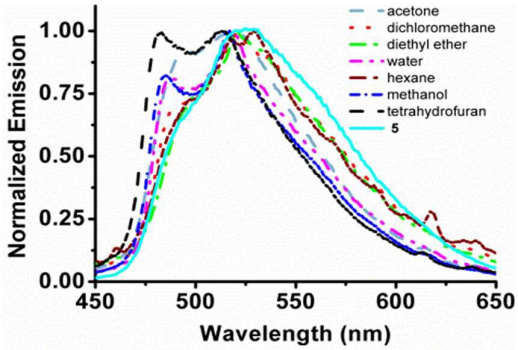

Fig. 9. Vapochromic emission responses of **5**.

Even though, no mechanochromic responses were detected from complexes featuring the pincer ligand of ^{MIC}(CNC)^{MIC}, they still exhibited vapochromic responses. Vapochromic behaviour of **5** and **6** are summarized in Fig. **9** and **10** respectively. Vapors of methanol, water, dichloromethane, and acetone transformed the weak emission shoulder of **5** at 493 nm into well-defined peaks. Distinct from other vapors, interaction of tetrahydrofuran with **5** induced largest blue shift. The peak at 530 nm reappeared at 513 nm, whereas the shoulder at 493 nm transformed into an intense band at 482 nm. As the new 482 nm became as intense as the 513 nm band, one could visualize the transformation of emission color from green to sky blue. Exposure of **6** to tetrahydrofuran, dichloromethane, water, methanol, diethyl ether, and hexane vapors resulted in the suppression of the shoulder at 550 nm with an exception of acetone that induced an intensity-gain and along with a slight bathochromic shift.

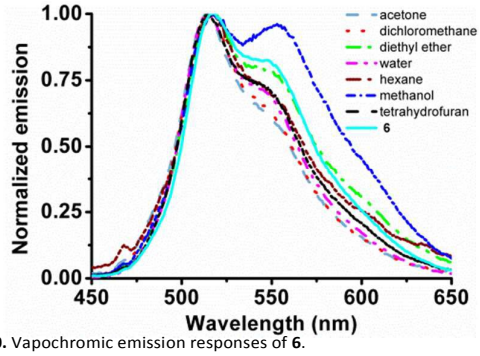

Fig. 10. Vapochromic emission responses of **6**.

Grinding induced red shift often arises due to the shortening of metallophilic contacts in planar platinum complexes.[4,8,13b,8,13d] However in complexes described herein, rather stronger secondary C–*H*···π and (or) hydrogen bonding interactions are detected (vide-supra). On these lines, amongst all of the complexes reported herein, the strongest mechanochromic response of $\Delta\lambda_{em}$ = 66 nm is exhibited by **2**. Nevertheless, the red shift in the emission and the accompanied transformation of less intense shoulders into a more intense-featureless band in **3** also correlates to short C–*H*···π contacts between the NHC donor and the mesityl ring. Similarly, the vapochromic response shown by **2**, bearing hydrogen bond donor sites of NHC backbone, coordinated acetonitrile and mesityl-methyl fragments is the strongest amongst these complexes. In general, one could attribute the vapochromic behaviour of **2**, **3**, **5** and **6** to vapor induced structural re-organization that could tickle the intermolecular C–*H*···π or the hydrogen bonding interactions.

Related vapor or pressure dependent color changes in platinum complexes bearing pure *N*-donors of terpyridine,[13a, 23a, 34] 1, 10-phenanthroline,[35] functionalized bipyridine[12f, 12g, 13c, 13d, 36] and hybrid *P*^*N* donor ligands[37] have been studied before. Incorporation of NHC donors in pincer motif into the coordination sphere of photo emissive platinum complex have shown to enhance the air and photo stability of the resultant triplet emitters.[38] However, difficulties related to their large-scale syntheses under inert atmospheres or manipulations of

toxic co-ligands like carbon monoxide have often hindered their application in functional materials. In this contribution, we have shown that the vapor/mechanochromic attributes of these complexes could be obtained even by using the weakly donating and readily accessible acetonitrile donors as the auxiliary ligands to the platinum centre.

Conclusions

Platinum complexes bearing pincer type-pyridine-*bis*-carbene ligands with normal imidazol-2-ylidene or mesoionic-triazol-5-ylidene as carbene donors are prepared. The latter complex introduced herein could be used as a valuable precursor to obtain several other platinum-based pincer luminophores. An aquachromic complex [$Pt^{NHC}(CNC)^{NHC}CO$] reported earlier was prepared *via* **1**, however its structural data which was not available then is also reported herein as **1**·PF_6 salt. A systematic variation of electronic environment at the platinum centre *via* substitution of −Cl auxiliary ligand of these parent complexes with $NCCH_3$ and CN donors afforded four more structurally distinct complexes. The observed trend in electrochemical redox potentials is in line with electron donor strength of pincer and auxiliary ligands, and the DFT computed relative orbital composition.

X-ray structures of four complexes show a distorted square-planar geometry with a twisted conformation between pincer ligands and mesityl fragments. Complexes featuring different pincer and auxiliary ligands exhibit distinct packing arrangement in the solid state showing varying degree of secondary CH−π and hydrogen bonding interactions. The platinum complex **1** and **4** bearing –Cl co-ligand did not exhibit vapochromic or mechanochromic responses. Complexes **5** and **6** featuring mesoionic-triazol-5-ylidene donors exhibited good vapochromic responses but no mechanochromic behaviour. **5** was found to be very sensitive to tetrahydrofuran vapor, as it showed a rapid emission response giving color changes from green to sky blue colors. Complexes **2** and **3** featuring the pyridine *bis*-imidazol-2-ylidene and an acetonitrile or cyano donors exhibited both of the photo functional attributes of vapochromism and mechanochromism. Sky blue emission color of **2** can either be switched into green upon exposure to different solvent vapors or to greenish-yellow upon grinding. Such visibly distinct emission responses of **2**, in combination with its easy large scale-accessibility are attractive for chemo sensing applications to detect volatile organic vapors and to sense mechanical shear in materials.

Experimental

Physical measurements and instrumentation.

Solvents and reagents are purchased from Sigma Aldrich. Acetonitrile and dichloromethane are purified by refluxing over calcium hydride on a standard solvent distillation set up. Other reagents are used as obtained, without further purification. NMR spectra were recorded on either a Bruker DPX-300 spectrometer (^{1}H-NMR, 299.96 MHz; ^{13}C-NMR, 75.43 MHz) or a Bruker AVANCE DPX-400 spectrometer (^{1}H, 400.13 MHz; ^{13}C, 100.61 MHz) using tetramethylsilane as an internal standard. Mass spectra were recorded on a Micromass Platform II spectrometer. Elemental microanalyses were performed at the Taiwan Instrumentation Center, Taipei.

UV-vis spectra are recorded on a Shimadzu UV-2101PC spectrophotometer. Emission spectra and the lifetimes are recorded on an Aminco Bowman AD 2 luminescence spectro-fluorometer. Cyclic voltammograms of complexes **1**, **2**, and **3** are recorded on a *BAS 100B* Electrochemical Analyzer, under a nitrogen atmosphere. The working, counter and the reference electrodes were glassy carbon, platinum foil and Ag/AgCl electrodes, respectively. All the electrochemical measurements were carried out at room temperature using dry-degassed acetonitrile solution containing 0.1M tetra butyl ammonium hexafluorophosphate. The standard concentration of analytes was ≈ 10^{-4}M and the optimal scan rate used was 0.1 V/s. Vapoluminescent behaviour of the complexes are probed from their crystals/powder samples deposited over a quartz plate placed in a closed chamber under the stream of respective vapors. Grinding of complexes using a mortar and pestle and subsequently recording the emission spectra facilitated the investigation of mechanochromic emission characteristics.

Single crystals of **1**·PF_6, **2**, **2**·H_2O, **3**·PF_6, and **4**·PF_6 suitable for X-ray diffraction were mounted over the tips of glass fibre with epoxy resin and subjected to X-ray diffraction. Data are collected on a Bruker APEX II diffractometer, using graphite monochromatic Mo Kα radiation (λ = 0.71073 Å). Data reduction was performed with SAINT, which corrects for Lorentz and polarization effects. Absorption corrections are performed using multiscan (SADABS). Structures were solved by using direct methods and refinement was performed by least-squares methods on F^2 using the SHELXL-97 package.[39] All H atoms are added in idealized positions. Solvent accessible voids were detected in **4**·PF_6, therefore, a SQUEEZE/PLATON[40] technique was applied to remove the unidentified solvent contributions. Crystals of **2**·H_2O were measured to support the vapochromic studies. Residual electron density in this structure is attributed to the aquachromic-deterioration of the quality of crystals.

Computational details.

DFT Calculations were performed using *Gaussian 09* package.[41] Ground state geometries of all the complexes were optimized by using the B3LYP[25] functional, with the SDD[26] basis set. The optimized structures were subjected to time dependent density-functional theory (TD-DFT) calculations to determine the vertical transition energies and oscillator strengths. The MO plots are obtained by using the *Gauss View 05* package.

Synthetic Procedures

1·PF_6: To a methanolic solution of **1**[12c] (0.71 g, 1 mmol) was added a solution of NH_4PF_6 (0.18 g, 1.1 mmol) in water (3 mL), and the mixture was stirred at ambient temperature for 15 minutes. Pale orange solid that precipitated over the clear supernatant solution was filtered off and dried *in vacuo* to obtain an analytically pure sample of **1**·PF_6 (0.66 g, 81%). ^{1}H NMR (300 MHz, acetone-d_6): δ 8.66 (t, J_{H-H} = 8.4 Hz, 1H), 8.56 (s, 2H), 8.15 (d, J_{H-H} = 8.4 Hz, 2H), 7.61 (s, 2H), 6.94 (s, 4H), 2.32 (s, 6H), 2.26 (s, 12 H) ppm. ^{13}C NMR (75 MHz, acetone-d_6): δ 168.9 (carbenoid-*C*), 152.3, 145.4, 139.3, 134.3, 133.7, 128.8, 125.6, 119.0, 108.3, 20.2 and 16.9 ppm. Mass (MALDI): m/*z* 678.3 $[M]^+$. *Anal. Calcd*. for $C_{29}H_{29}ClF_6N_5PPt$: C 42.32; H 3.55; N 8.51. Found: C 42.27; H 3.55; N 7.85.

2: A mixture of **1** (0.71 g, 1.0 mmol) and $AgPF_6$ (0.53 g, 2.1 mmol) was stirred in acetonitrile (20 mL) at ambient temperature for 1 h. During this time, precipitation of colorless solids was observed (AgCl). Separation of the yellow supernatant solution over a bed of celite and subsequent addition of diethyl ether (20 mL) gave yellow powder of **2** (0.71 g, 73 %). ^{1}H NMR (300 MHz, acetone-

d_6): δ 8.63 (s, 2H), 8.72 (t, J_{H-H} = 8.4 Hz, 1H), 8.24 (d, J_{H-H} = 8.4 Hz, 2H), 7.82 (s, 2H), 7.14 (s, 4H), 2.31 (s, 6H), 2.12 (s, 12 H), 1.82 (s, 3H). ^{13}C NMR (75 MHz, acetone-d_6): δ 166.8 (carbenoid-*C*), 153.0, 148.6, 140.7, 135.1, 133.3, 129.5, 125.1, 120.5, 109.3, 118.5, 20.1, and 0.5 ppm. Mass (MALDI): m/*z* 828.7 $[M+PF_6]^+$. *Anal. Calcd*. for $C_{31}H_{32}ClF_{12}N_6P_2Pt{\cdot}0.5\ CH_3(CO)CH_3$: C 38.93; H 3.52; N 8.38. Found: C 38.97; H 3.57; N 8.58.

3: A mixture of **1** (0.3 g, 0.04 mmol) and AgCN (5.3 mg, 0.04 mmol) in 1 mL of dichloromethane was stirred at ambient temperature for 12 h. After this time, the solvent was removed on a rotary evaporator to obtain the crude product. Further washing of the crude with diethyl ether and subsequent drying under high vacuum afforded **3** (24 mg, 81%) as yellow solids. ^{1}H NMR (300 MHz, acetonitrile-d_3): δ 8.47 (t, J_{H-H} = 7.4 Hz, 1H), 8.21 (s, 2H), 7.91 (d, J_{H-H} = 7.4 Hz), 7.31 (s, 2H), 6.99 (s, 4H), 2.28 (s, 6H) and 2.04 (s, 12H) ppm. ^{13}C NMR (75 MHz, acetonitrile-d_3): δ 169.4 (carbenoid-*C*), 156.6, 152.2, 147.4, 140.1, 134.3, 133.9, 129.1, 124.8, 119.9, 108.7, 20.2, 17.0 ppm. Mass (MALDI): m/*z* 667.2 $[M+1]^+$. IR: 2143 cm^{-1} (–CN). *Anal. Calcd*. for $C_{30}H_{29}N_6ClPt$: C 51.17; H 4.15; N 11.94. Found: C 51.05; H 4.28; N 11.94. In order to obtain the X-ray quality crystals, the –Cl counter ion was exchanged with PF_6 using NH_4PF_6 by following a similar procedure as described for **1**·PF_6. *Anal. Calcd*. for $C_{30}H_{29}F_6N_6PPt{\cdot}5{\cdot}H_2O$: C 39.87; H 4.35; N 9.30. Found: C 39.82; H 4.08; N 9.09.

4: An acetonitrile solution of (^{Mes}CNC^{Mes})–$H_2[BF_4]_2$ [9b, 42] (0.40 g, 0.61mmol) was added to an aqueous solution of K_2PtCl_4 (290 mg, 0.70mmol). The reaction mixture was stirred at ambient temperature for 3 h and then filtered. Subsequent drying *in vacuo* gave (^{Mes}CNC^{Mes})–$H_2[PtCl_4]$ (0.40 g, 0.54 mmol, 88%) as a pink powder. This intermediate salt was characterized by ^{1}H and ^{13}C NMR, and used as such for the subsequent reaction. (^{Mes}CNC^{Mes})–$H_2[PtCl_4]$:^{1}H NMR (300 MHz, DMSO-d_6): δ 10.01 (s, 2H), 8.48 (m, 3H), 7.26 (m, 4H), 4.77 (s, 6H), 2.39 (s, 6H), 2.16 (s, 12H). ^{13}C NMR (101 MHz, DMSO-d_6): δ 143.5, 142.2, 140.5, 140.4, 134.5, 132.9, 131.1 (C^5), 129.6, 126.8, 41.6, 20.8, 16.9. To a suspension of (^{Mes}CNC^{Mes})–$H_2[PtCl_4]_2$ salt (0.35 g, 0.54 mmol) in 15 mL DMSO was added Ag_2O (134 mg, 0.58 mmol). The mixture was heated at 140 °C for 10 h to yield an orange solution. After this time, the orange solution was cooled to ambient temperature. Dichloromethane was added to the reaction mixture and the organic layer was washed with brine (×3 times). Removal of dichloromethane *in vacuo*, gave the crude product, which was further purified by column chromatography (aluminoxide, MeOH/DCM = 1:9 (*V*/*V*)) to obtain an analytically pure form of **4** as yellow powder (65 mg, 16.1%). ^{1}H NMR (300 MHz, $CDCl_3$): δ 8.44 (t, *J* = 8.0 Hz, 1H), 8.04 (d, *J* = 8.0 Hz, 2H), 7.17 (s, 4H), 4.69 (s, 6H), 2.48 (s, 6H), 2.25 (s, 12H) ppm. ^{13}C NMR (75 MHz, CD_3CN): δ 164.2, 152.2 (d, *J* = 13.5 Hz), 143.0, 141.7, 136.0 (d, *J* = 11.0 Hz), 135.5, 134.8, 129.6, 120.6, 39.8, 21.1, 17.5 ppm. Mass (MALDI): m/*z* = 708.1 $[M^+]$, m/*z* = 672.1 $[M-Cl]^+$. *Anal. Calcd. For* $C_{29}H_{29}Cl_2N_5Pt$: C 46.84; H 3.75; N 13.19; Found: C 47.50; H 3.67; N 12.93.

5: A mixture of **4** (50mg, 0.07mmol) and $AgPF_6$ (1.8mg, 0.07mmol) in acetonitrile was stirred at ambient temperature for 12 h. After this time, the reaction mixture was filtered off. The filtrate was evaporated in rotary evaporator, residue was washed with diethyl ether and finally dried in high vacuum to obtain **5** (49mg, 86%) as yellow powder. ^{1}H NMR (300 MHz, acetone-d_6): δ 8.42 (t, J_{H-H} = 7.96 Hz, 1H), 8.16 (d, J_{H-H} = 7.96, 2H), 7.17 (s, 4H), 4.80 (s, 6H), 2.33 (s, 6H), 2.07 (s, 12H), 1.30 (s, 3H) ppm. ^{13}C NMR (75 MHz, acetone-d_6) δ 161.9, 153.4, 152.5, 146.1, 142.6, 135.8, 134.1, 130.3, 129.9 (d, *J* = 6.64 Hz), 121.9, 40.1, 21.0, 17.4, 2.6 ppm. Mass (MALDI): m/*z* = 672.3 $[M-CH_3CN]^{2+}$. *Anal. Calcd. For* $C_{31}H_{34}F_{12}N_8P_2Pt{\cdot}6{\cdot}CH_2Cl_2{\cdot}1.5{\cdot}CH_3CN$: C 30.51; H 3.23; N 8.45; Found: C 30.61; H 3.23; N 8.76.

6: A mixture of **4** (30mg, 0.04mmol) and AgCN (5.3mg, 0.04mmol) in dichloromethane (1 mL) was stirred at ambient temperature for 12 h. After this time, solvent was removed on a rotary evaporator and the crude was triturated with diethyl ether and subsequently dried in high vacuum, to obtain yellow powders of **6** (24mg, 81%). ^{1}H NMR (300 MHz, acetone-d_6): δ 8.39 (t, J_{H-H} = 8.00 Hz, 1H), 8.16 (d, J_{H-H} = 8.00, 2H), 7.06 (s, 4H), 4.77 (s, 6H), 2.35 (s, 6H), 2.13 (s, 12H) ppm. ^{13}C NMR (75 MHz, acetone-d_6) δ 164.6, 153.5, 152.4, 144.9 (*C*N), 141.5, 135.6, 135.2, 134.8, 130.0, 121.2, 39.9, 21.3, 17.8 ppm. Mass (MALDI): m/*z* = 732.2 $[M]^+$, m/*z* = 672.1 $[M-CN]^+$. IR: 2131.0 cm^{-1} (–CN). *Anal. Calcd. For* $C_{30}H_{31}F_6N_8PPt{\cdot}0.5{\cdot}CH_3CN{\cdot}CH_3(CO)CH_3{\cdot}\ 2{\cdot}H_2O$: C 42.61; H 4.47; N 12.42; Found: C 42.88; H 4.22; N 12.72.

Acknowledgments

Authors thank the Ministry of Science and Technology Taiwan for financially supporting this project.

Notes and references

1. (a) S. Díez-González, N. Marion and S. P. Nolan, *Chem. Rev.*, 2009, **109**, 3612–3676; (b) A. R. Naziruddin, C. S. Zhuang, W. J. Lin and W. S. Hwang, *Dalton Trans.*, 2014, **43**, 5335–5342; (c) A. R. Naziruddin, Z. J. Huang, W. C. Lai, W. J. Lin and W. S. Hwang, *Dalton Trans.*, 2013, **42**, 13161–13171; (d) J. A. Loch, M. Albrecht, E. Peris, J. Mata, J. W. Faller and R. H. Crabtree, *Organometallics*, 2002, **21**, 700–706; (e) A. A. Danopoulos, S. Winston and W. B. Motherwell, *Chem. Commun.*, 2002, 1376–1377; (f) J. A. Wright, A. A. Danopoulos, W. B. Motherwell, R. J. Carroll and S. Ellwood, *J. Organomet. Chem.*, 2006, **691**, 5204–5210; (g) A. A. Danopoulos, D. Pugh and J. A. Wright, *Angew. Chem. Int. Ed.*, 2008, **47**, 9765–9767; (h) A. A. Danopoulos, D. Pugh, H. Smith and J. Saßmannshausen, *Chem. Eur. J.*, 2009, **15**, 5491–5502; (i) F. E. Hahn, M. C. Jahnke and T. Pape, *Organometallics*, 2006, **25**, 5927–5936.
2. L. Mercs and M. Albrecht, *Chem. Soc. Rev.*, 2010, **39**, 1903–1912.
3. M. Mauro, A. Aliprandi, D. Septiadi, N. S. Kehr and L. De Cola, *Chem. Soc. Rev.*, 2014, **43**, 4144–4166.
4. (a) K. Farrell and M. Albrecht, in *The Privileged Pincer-Metal Platform: Coordination Chemistry & Applications*, eds. G. van Koten and A. R. Gossage, Springer International Publishing, Cham, 2016, 45-91; (b) V. W. Yam, V. K. Au and S. Y. Leung, *Chem. Rev.*, 2015, **115**, 7589–7728.
5. Y. Kawamura, K. Goushi, J. Brooks, J. J. Brown, H. Sasabe and C. Adachi, *Appl. Phys. Lett.*, 2005, **86**, 71104.
6. (a) A. Y.-Y. Tam, D. P.-K. Tsang, M.-Y. Chan, N. Zhu and V. W.-W. Yam, *Chem. Commun.*, 2011, **47**, 3383-3385; (b) E. S.-H. Lam, D. P.-K. Tsang, W. H. Lam, A. Y.-Y. Tam, M.-Y. Chan, W.-T. Wong and V. W.-W. Yam, *Chem. Eur. J.*, 2013, **19**, 6385–6397; (c) R. Visbal and M. C. Gimeno, *Chem. Soc.*

Rev., 2014, **43**, 3551–3574; (d) N. Darmawan, C.-H. Yang, M. Mauro, M. Raynal, S. Heun, J. Pan, H. Buchholz, P. Braunstein and L. De Cola, *Inorg. Chem.*, 2013, **52**, 10756–10765; (e) A. R. Naziruddin, A. Galstyan, A. Iordache, C. G. Daniliuc, C. A. Strassert and L. De Cola, *Dalton Trans.*, 2015, **44**, 8467–8477; (f) C. H. Yang, J. Beltran, V. Lemaur, J. Cornil, D. Hartmann, W. Sarfert, R. Frohlich, C. Bizzarri and L. De Cola, *Inorg. Chem.*, 2010, **49**, 9891–9901; (g) M. Tenne, S. Metz, I. Münster, G. Wagenblast and T. Strassner, *Organometallics*, 2013, **32**, 6257–6264; (h) Y. Unger, D. Meyer, O. Molt, C. Schildknecht, I. Münster, G. Wagenblast and T. Strassner, *Angew. Chem. Int. Ed.*, 2010, **49**, 10214–10216; (i) Y. Unger, D. Meyer and T. Strassner, *Dalton Trans.*, 2010, **39**, 4295–4301; (j) Y.-C. Chiu, Y. Chi, J.-Y. Hung, Y.-M. Cheng, Y.-C. Yu, M.-W. Chung, G.-H. Lee, P.-T. Chou, C.-C. Chen, C.-C. Wu and H.-Y. Hsieh, *ACS Appl. Mater. Interfaces*, 2009, **1**, 433–442.

7. (a) M. Albrecht, in *Adv. Organomet. Chem.*, ed. J. P. Pedro, Academic Press, 2014, vol. Volume 62, 111–158; (b) Y. Zhang, J. Clavadetscher, M. Bachmann, O. Blacque and K. Venkatesan, *Inorg. Chem.*, 2014, **53**, 756–771.
8. W.-J. Lin, A. R. Naziruddin, Y.-H. Chen, B.-J. Sun, A. H. H. Chang, W.-J. Wang and W.-S. Hwang, *Chem. Asian J.*, 2015, **10**, 728–739.
9. (a) K. Farrell and M. Albrecht, Late Transition Metal Complexes with Pincer Ligands that Comprise N-Heterocyclic Carbene Donor Sites, Springer Berlin Heidelberg, **2015**, 1–47; (b) D. G. Brown, N. Sanguantrakun, B. Schulze, U. S. Schubert and C. P. Berlinguette, *J. Am. Chem. Soc.*, 2012, **134**, 12354–12357; (c) A. R. Naziruddin, C.-L. Kuo, W.-J. Lin, W.-H. Lo, C.-S. Lee, B.-J. Sun, A. H. H. Chang and W.-S. Hwang, *Organometallics*, 2014, **33**, 2575–2582; (d) K. K.-W. Lo, A. W.-T. Choi and W. H.-T. Law, *Dalton Trans.*, 2012, **41**, 6021–6047; (e) T. C. Johnstone, J. J. Wilson and S. J. Lippard, *Inorg. Chem.*, 2013, **52**, 12234–12249; (f) T. Banerjee, P. Dubey and R. Mukhopadhyay, *Biochimie*, 2010, **92**, 846–851; (g) R. G. Alabau, B. Eguillor, J. Esler, M. A. Esteruelas, M. Oliván, E. Oñate, J.-Y. Tsai and C. Xia, *Organometallics*, 2014, **33**, 5582-5596; (h) L.-H. Chung, S.-C. Chan, W.-C. Lee and C.-Y. Wong, *Inorg. Chem.*, 2012, **51**, 8693-8703; (i) S. Sinn, B. Schulze, C. Friebe, D. G. Brown, M. Jäger, E. Altuntaş, J. Kübel, O. Guntner, C. P. Berlinguette, B. Dietzek and U. S. Schubert, *Inorg. Chem.*, 2014, **53**, 2083-2095.
10. (a) C.-K. Koo, Y.-M. Ho, C.-F. Chow, M. H.-W. Lam, T.-C. Lau and W.-Y. Wong, *Inorg. Chem.*, 2007, **46**, 3603–3612; (b) Z. He, W.-Y. Wong, X. Yu, H.-S. Kwok and Z. Lin, *Inorg. Chem.*, 2006, **45**, 10922–10937; (c) W.-Y. Wong, Z. He, S.-K. So, K.-L. Tong and Z. Lin, *Organometallics*, 2005, **24**, 4079–4082; (d) A. Galstyan, A. R. Naziruddin, C. Cebrián, A. Iordache, C. G. Daniliuc, L. De Cola and C. A. Strassert, *Eur. J. Inorg. Chem.*, 2015, 5822–5831.
11. (a) K. Li, Y. Chen, W. Lu, N. Zhu and C.-M. Che, *Chem. Eur. J.*, 2011, **17**, 4109–4112; (b) K. Li, T. Zou, Y. Chen, X. Guan and C.-M. Che, *Chem. Eur. J.*, 2015, **21**, 7441–7453.
12. (a) F. Nastasi, F. Puntoriero, N. Palmeri, S. Cavallaro, S. Campagna and S. Lanza, *Chem. Commun.*, 2007, 4740–4742; (b) C.-S. Lee, S. Sabiah, J.-C. Wang, W.-S. Hwang and I. J. B. Lin, *Organometallics*, 2010, **29**, 286–289; (c) C.-S. Lee, R. R. Zhuang, S. Sabiah, J.-C. Wang, W.-S. Hwang and I. J. B. Lin, *Organometallics*, 2011, **30**, 3897–3900; (d) Y. Chen, W. Lu and C.-M. Che, *Organometallics*, 2012, **32**, 350–353; (e) J. Moussa, K. M.-C. Wong, X. F. Le Goff, M. N. Rager, C. K.-M. Chan, V. W.-W. Yam and H. Amouri, *Organometallics*, 2013, **32**, 4985–4992; (f) J. Ni, Y.-G. Wang, J.-Y. Wang, Y.-Q. Zhao, Y.-Z. Pan, H.-H. Wang, X. Zhang, J.-J. Zhang and Z.-N. Chen, *Dalton Trans.*, 2013, **42**, 13092–13100; (g) X. Zhang, J.-Y. Wang, J. Ni, L.-Y. Zhang and Z.-N. Chen, *Inorg. Chem.*, 2012, **51**, 5569–5579.
13. (a) P. Du, J. Schneider, W. W. Brennessel and R. Eisenberg, *Inorg. Chem.*, 2007, **47**, 69–77; (b) A. Han, P. Du, Z. Sun, H. Wu, H. Jia, R. Zhang, Z. Liang, R. Cao and R. Eisenberg, *Inorg. Chem.*, 2014, **53**, 3338–3344; (c) J. Ni, X. Zhang, Y.-H. Wu, L.-Y. Zhang and Z.-N. Chen, *Chem. Eur. J.*, 2011, **17**, 1171–1183; (d) J. Ni, X. Zhang, N. Qiu, Y.-H. Wu, L.-Y. Zhang, J. Zhang and Z.-N. Chen, *Inorg. Chem.*, 2011, **50**, 9090–9096; (e) J. Schneider, Y.-A. Lee, J. Pérez, W. W. Brennessel, C. Flaschenriem and R. Eisenberg, *Inorg. Chem.*, 2008, **47**, 957–968; (f) Y.-A. Lee and R. Eisenberg, *J. Am. Chem. Soc.*, 2003, **125**, 7778–7779.
14. M. Albrecht, *Science*, 2009, **326**, 532-533.
15. V. Khlebnikov, M. Heckenroth, H. Muller-Bunz and M. Albrecht, *Dalton Trans.*, 2013, **42**, 4197-4207.
16. P. Mathew, A. Neels and M. Albrecht, *J. Am. Chem. Soc.*, 2008, **130**, 13534-13535.
17. D. Mendoza-Espinosa, R. González-Olvera, G. E. Negrón-Silva, D. Angeles-Beltrán, O. R. Suárez-Castillo, A. Álvarez-Hernández and R. Santillan, *Organometallics*, 2015, **34**, 4529-4542.
18. (a) J. D. Crowley, A.-L. Lee and K. J. Kilpin, *Aust. J. Chem.*, 2011, **64**, 1118–1132; (b) E. M. Schuster, M. Botoshansky and M. Gandelman, *Dalton Trans.*, 2011, **40**, 8764–8767.
19. R. Maity, T. Tichter, M. van der Meer and B. Sarkar, *Dalton Trans.*, 2015, **44**, 18311–18315.
20. B. Schulze, D. Escudero, C. Friebe, R. Siebert, H. Görls, U. Köhn, E. Altuntas, A. Baumgaertel, M. D. Hager, A. Winter, B. Dietzek, J. Popp, L. González and U. S. Schubert, *Chem. Eur. J.*, 2011, **17**, 5494–5498.
21. D. I. Bezuidenhout, G. Kleinhans, G. Guisado-Barrios, D. C. Liles, G. Ung and G. Bertrand, *Chem. Commun.*, 2014, **50**, 2431–2433.
22. (a) V. Khlebnikov, M. Heckenroth, H. Muller-Bunz and M. Albrecht, *Dalton Transactions*, 2013, **42**, 4197-4207; (b) H. Jin, T. T. Tan and F. E. Hahn, *Angew. Chem. Int. Ed.*, 2015, **54**, 13811–13815.
23. (a) R. Zhang, Z. Liang, A. Han, H. Wu, P. Du, W. Lai and R. Cao, *CrystEngComm*, 2014, **16**, 5477–5742; (b) V. W.-W. Yam, R. P.-L. Tang, K. M.-C. Wong and K.-K. Cheung, *Organometallics*, 2001, **20**, 4476–4482.
24. J. D. Dunitz and R. Taylor, *Chem. Eur. J.*, 1997, **3**, 89–98.
25. (a) A. D. Becke, *J. Chem. Phys*, 1993, **98**, 5648–5652; (b) C. Lee, W. Yang and R. G. Parr, *Phys Rev B*, 1988, **37**, 785–789.
26. (a) D. Andrae, U. Häußermann, M. Dolg, H. Stoll and H. Preuß, *Theoret. Chim. Acta*, 1990, **77**, 123–141; (b) A. Bergner, M. Dolg, W. Küchle, H. Stoll and H. Preuß, *Mol. Phys.*, 1993, **80**, 1431–1441; (c) D. Figgen, K. A. Peterson, M. Dolg and H. Stoll, *J. Chem. Phys.*, 2009, **130**, 164108.
27. A. Colombo, F. Fiorini, D. Septiadi, C. Dragonetti, F. Nisic, A. Valore, D. Roberto, M. Mauro and L. De Cola, *Dalton Trans.*, 2015, **44**, 8478–8487.
28. J. A. G. Williams, A. Beeby, E. S. Davies, J. A. Weinstein and C. Wilson, *Inorg. Chem.*, 2003, **42**, 8609–8611.

29. V. Leigh, W. Ghattas, R. Lalrempuia, H. Müller-Bunz, M. T. Pryce and M. Albrecht, *Inorg. Chem.*, 2013, **52**, 5395–5402.
30. (a) S. Y.-L. Leung, E. S.-H. Lam, W. H. Lam, K. M.-C. Wong, W.-T. Wong and V. W.-W. Yam, *Chem. Eur. J.*, 2013, **19**, 10360–10369; (b) V. W.-W. Yam, K. H.-Y. Chan, K. M.-C. Wong and N. Zhu, *Chem. Eur. J.*, 2005, **11**, 4535–4543; (c) A. Y.-Y. Tam, W. H. Lam, K. M.-C. Wong, N. Zhu and V. W.-W. Yam, *Chem. Eur. J.*, 2008, **14**, 4562–4576.
31. M. G. Hill, J. A. Bailey, V. M. Miskowski and H. B. Gray, *Inorg. Chem.*, 1996, **35**, 4585–4590.
32. V. W.-W. Yam and K. M.-C. Wong, *Chem. Commun.*, 2011, **47**, 11579–11592.
33. S.-W. Lai, M. C.-W. Chan, K.-K. Cheung and C.-M. Che, *Organometallics*, 1999, **18**, 3327–3336.
34. (a) V. W.-W. Yam, K. M.-C. Wong and N. Zhu, *J. Am. Chem. Soc.*, 2002, **124**, 6506–6507; (b) T. J. Wadas, Q.-M. Wang, Y.-j. Kim, C. Flaschenreim, T. N. Blanton and R. Eisenberg, *J. Am. Chem. Soc.*, 2004, **126**, 16841–16849; (c) W. Lu, Y. Chen, V. A. L. Roy, S. S.-Y. Chui and C.-M. Che, *Angew. Chem. Int. Ed.*, 2009, **48**, 7621–7625.
35. J. Ni, J.-J. Kang, H.-H. Wang, X.-Q. Gai, X.-X. Zhang, T. Jia, L. Xu, Y.-Z. Pan and J.-J. Zhang, *RSC Advances*, 2015, **5**, 65613–65617.
36. T. Ohba, A. Kobayashi, H.-C. Chang and M. Kato, *Dalton Trans.*, 2013, **42**, 5514–5523.
37. L. J. Grove, A. G. Oliver, J. A. Krause and W. B. Connick, *Inorg. Chem.*, 2008, **47**, 1408–1410.
38. X. Zhang, A. M. Wright, N. J. DeYonker, T. K. Hollis, N. I. Hammer, C. E. Webster and E. J. Valente, *Organometallics*, 2012, **31**, 1664–1672.
39. (a) G. Sheldrick, *Acta Cryst. A,*, 2008, **64**, 112–122; (b) G. Sheldrick, *Acta Crystallogr A*, 1990, **46**, 467–473; (c) G. M. Sheldrick, *Acta Cryst. A,*, 2008, **64**, 112–122.
40. A. Spek, *J. Appl. Crystallogr.*, 2003, **36**, 7–13.
41. M. J. Frisch, G. W. Trucks, H. B. Schlegel, G. E. Scuseria, M. A. Robb, J. R. Cheeseman, G. Scalmani, V. Barone, B. Mennucci, G. A. Petersson, H. Nakatsuji, M. Caricato, X. Li, H. P. Hratchian, A. F. Izmaylov, J. Bloino, G. Zheng, J. L. Sonnenberg, M. Hada, M. Ehara, K. Toyota, R. Fukuda, J. Hasegawa, M. Ishida, T. Nakajima, Y. Honda, O. Kitao, H. Nakai, T. Vreven, J. A. Montgomery, Jr., J. E. Peralta, F. Ogliaro, M. Bearpark, J. J. Heyd, E. Brothers, K. N. Kudin, V. N. Staroverov, R. Kobayashi, J. Normand, K. Raghavachari, A. Rendell, J. C. Burant, S. S. Iyengar, J. Tomasi, M. Cossi, N. Rega, J. M. Millam, M. Klene, J. E. Knox, J. B. Cross, V. Bakken, C. Adamo, J. Jaramillo, R. Gomperts, R. E. Stratmann, O. Yazyev, A. J. Austin, R. Cammi, C. Pomelli, J. W. Ochterski, R. L. Martin, K. Morokuma, V. G. Zakrzewski, G. A. Voth, P. Salvador, J. J. Dannenberg, S. Dapprich, A. D. Daniels, O. Farkas, J. B. Foresman, J. V. Ortiz, J. Cioslowski and D. J. Fox, Gaussian 09, Revision D.01, edn., 2009, , vol. Gaussian.
42. J. P. Byrne, J. A. Kitchen, O. Kotova, V. Leigh, A. P. Bell, J. J. Boland, M. Albrecht and T. Gunnlaugsson, *Dalton Trans.*, 2014, **43**, 196–209.

For TOC Graphics:

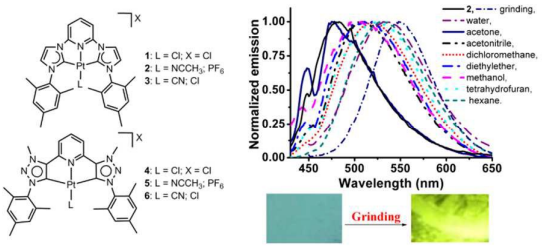

Platinum Complexes featuring pyridine *bis*-*N*-heterocyclic imidazol-2-ylidene or triazol-5-ylidene are prepared with different auxiliary ligands. This report summarizes their structures, photo-physics and electrochemical details. Vapo/mechanochromic emission responses have also been detected.